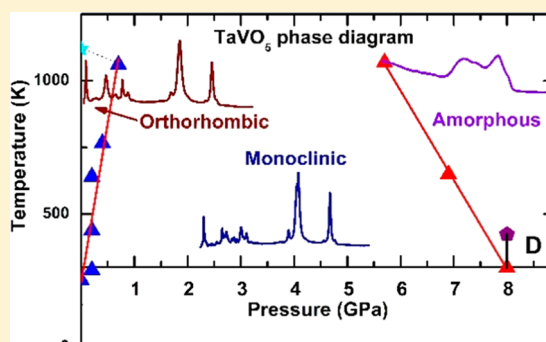


# High Pressure Phases and Amorphization of a Negative Thermal Expansion Compound TaVO<sub>5</sub>

Nilesh P. Salke,<sup>†,‡</sup> Rekha Rao,<sup>\*,†,‡</sup> Srungarpu Nagabhusan Achary,<sup>‡,§</sup> Chandrani Nayak,<sup>§</sup> Alka B. Garg,<sup>||,¶</sup> P. S. R. Krishna,<sup>†</sup> A. B. Shinde,<sup>†</sup> Shambu Nath Jha,<sup>§</sup> Dibyendu Bhattacharyya,<sup>§</sup> Jagannath,<sup>⊥</sup> and Avesh Kumar Tyagi<sup>‡</sup>

<sup>†</sup>Solid State Physics Division, <sup>‡</sup>Chemistry Division, <sup>§</sup>Atomic and Molecular Physics Division, <sup>||</sup>High Pressure and Synchrotron Radiation Physics Division, and <sup>⊥</sup>Technical Physics Division, Bhabha Atomic Research Centre, Mumbai-400085, India

**ABSTRACT:** Negative thermal expansion material TaVO<sub>5</sub> is recently reported to have pressure induced structural phase transition and irreversible amorphization at 0.2 and above 8 GPa, respectively. Here, we have investigated the high pressure phase of TaVO<sub>5</sub> using *in situ* neutron diffraction studies. The first high pressure phase is identified to be monoclinic *P*<sub>2</sub><sub>1</sub>/*c* phase, same as the low temperature phase of TaVO<sub>5</sub>. On heating, amorphous TaVO<sub>5</sub> transformed to a new crystalline phase, which showed signatures of higher coordination of vanadium indicating pressure induced amorphization (PIA). PIA observed in TaVO<sub>5</sub> might be due to the kinetic hindrance of pressure induced decomposition (PID) into a compound with higher coordination of vanadium. Mechanism of PIA observed in TaVO<sub>5</sub> is investigated by carrying out *ex situ* Raman, XRD, XPS, and XAS measurements. We have also proposed a pressure–temperature phase diagram of TaVO<sub>5</sub> qualitatively delineating the phase boundaries between the ambient orthorhombic, monoclinic, and amorphous phases.



## INTRODUCTION

Since the first discovery of pressure induced amorphization (PIA) in ice, there has been great interest in PIA, which is observed in a wide variety of materials.<sup>1–4</sup> PIA is interesting due to its anomalous nature, as under pressure amorphous materials are expected to crystallize.<sup>5,6</sup> The mechanism responsible for these phenomena is different in different classes of materials. Thermodynamic melting is one of the mechanisms known to result in amorphization when a crystalline solid is compressed beyond its extrapolated melting curve.<sup>1</sup> PIA is also understood as a phenomenon of uncorrelated tilting of the polyhedral units resulting in an amorphous phase or orientationally disordered in some cases. Changes in the atomic coordination to have better packing also has been considered to contribute to PIA.<sup>7</sup> The other possibilities include amorphization due to insufficient kinetics essential for equilibrium structural phase transition/decomposition.<sup>1</sup> In most such cases the high pressure phase or decomposed products remain unknown. There are several reports on PIA and its mechanism;<sup>6–8</sup> particularly, PIA observed in ice, quartz, berlinite, etc., are a few pioneering examples in this field.<sup>9–11</sup> Recently, it has also been reported for vanadates and molybdates.<sup>12–14</sup> Some amorphous materials are reported to have memory effect as they regain the structure after decompression,<sup>8</sup> e.g., clathrate hydrates in which network structure remains intact, in collapsed structure due to unbroken bonds, which helps to retain original structure after decompression.<sup>8</sup> PIA was also found to be reversible in some

cases such as CaWO<sub>4</sub>.<sup>15</sup> Polymorphic forms of amorphous materials known as “polyamorphism” has also been investigated, and it is noticed that amorphous phases could be different based on density, coordination number, entropy, composition, etc.<sup>16–20</sup> These variations subsequently alter the electronic and vibrational properties of polyamorphic forms.

Materials with negative thermal expansion (NTE) coefficient are also well-known for their interesting high pressure phase transition behavior, and PIA is observed often at relatively lower pressures;<sup>2,3</sup> which suggest a common link between PIA and NTE.<sup>3</sup> ZrW<sub>2</sub>O<sub>8</sub>, Ag<sub>3</sub>Co(CN)<sub>6</sub>, many tungstates, and molybdates have been studied extensively for their high pressure phase transitions, and PIA is observed in all of them.<sup>2,21,22</sup> Several mechanisms have been proposed for the PIA in ZrW<sub>2</sub>O<sub>8</sub>. High pressure Raman and XRD studies attributed the tilting and deformation of ZrO<sub>6</sub> and WO<sub>4</sub> polyhedral groups to PIA.<sup>21</sup> Later, high pressure X-ray absorption spectroscopy (XAS) studies suggested the increase in the Zr and W coordination number in the amorphous phase of ZrW<sub>2</sub>O<sub>8</sub>, which is in contradiction to the earlier proposed tilting and deformation mechanism for PIA.<sup>22,23</sup> PIA in ZrW<sub>2</sub>O<sub>8</sub> is also evidenced to be due to kinetic hindrance of pressure induced decomposition (PID). PIA in cyanides has been attributed to the kinetic hindrance for decomposition.<sup>24,25</sup> In metavanadates, PIA is associated with breaking up of cross-

Received: March 13, 2018

Published: June 7, 2018

linked tetrahedral  $\text{VO}_4$  chains into  $\text{VO}_3^{-1}$ , and the original crystalline phase is recovered when the pressure amorphous material is heated.<sup>12</sup> As vanadium can exist in multiple oxidation states, which can change easily under pressure, vanadates tend to transform into the phases with higher coordination of vanadium atom under pressure, which could force them into amorphous phase due to lack of kinetics.<sup>26</sup>

Recently,  $\text{TaVO}_5$  belonging to  $\text{ABO}_5$  family is reported to have volumetric NTE behavior above room temperature.<sup>27</sup>  $\text{TaVO}_5$  is orthorhombic at room temperature and speculated to transform into tetragonal phase above 873 K.<sup>27</sup> X-ray diffraction (XRD) and powder neutron diffraction measurements on  $\text{TaVO}_5$  have reported reversible transition to a monoclinic phase below 259 K.<sup>27</sup> There are a few reports of PIA in components,  $\text{Ta}_2\text{O}_5$  in the nanophase<sup>28</sup> as well as bulk<sup>29</sup> and  $\text{V}_2\text{O}_5$ .<sup>19</sup> High pressure Raman spectroscopic studies on  $\text{TaVO}_5$  have reported a reversible structural phase transition at 0.2 GPa and an irreversible PIA above 8 GPa.<sup>30</sup> Though the high pressure phase is unknown, from Raman measurements it is speculated to be monoclinic.<sup>30</sup> In this Article, we report our high pressure neutron diffraction investigation on  $\text{TaVO}_5$  to identify the structure of its high pressure phase. We have carried out *ex situ* Raman, XRD, X-ray photoelectron spectroscopy (XPS), and XAS measurements on pressure retrieved  $\text{TaVO}_5$  to identify the nature of PIA observed. In addition, we have explored pressure–temperature phase relation in the temperature range 77–1100 K and up to 8 GPa.

## EXPERIMENTAL DETAILS

$\text{TaVO}_5$  was synthesized by solid-state reaction method from a stoichiometric mixture of  $\text{Ta}_2\text{O}_5$  and  $\text{V}_2\text{O}_5$ , following the procedure given in ref 26, and characterized by XRD using  $1.54 \text{ \AA}$  of  $\text{Cu K}\alpha$ .

The high pressure neutron diffraction studies on  $\text{TaVO}_5$  were done using a compact end loaded piston cylinder press, which can be used up to 2.5 GPa for neutron diffraction studies on large sample volume. The pressure chamber is made up of hardened EN45 steel.<sup>31</sup> Neutron diffraction studies were carried out on  $\text{TaVO}_5$  polycrystalline sample without any pressure transmitting medium, at various pressures from ambient pressure up to 0.5 GPa pressure using this previously calibrated pressure cell. The diffraction measurements were carried out on the High-Q diffractometer at Dhruva reactor, BARC, Mumbai, using neutrons of wavelength  $1.278 \text{ \AA}$ .<sup>32</sup> The data was then corrected for absorption, multiple scattering, and cell background using the methods given by Petrillo et al.<sup>33</sup> for thick cells. The data obtained in between the first two Bragg peaks of the pressure cell have been used for presentation and Rietveld analysis. Essentially the contribution in this  $2\theta$  range is from the sample only.

Raman spectra were excited using 532 nm laser focused to a spot size of  $20 \mu\text{m}$ . High pressure measurements were carried out from inside a diamond anvil cell Diacell B-05 and membrane diamond anvil cell (OMNI-DAC LT of Almax-Easylab, UK) with a 4:1 methanol–ethanol mixture as the pressure transmitting medium, which remains hydrostatic up to 10.4 GPa and quasi-hydrostatic up to 20 GPa.<sup>34</sup> Pressure was measured using the ruby fluorescence technique.<sup>35</sup> Scattered light was analyzed using a home-built 0.9 m single monochromator, coupled with an edge filter and detected by a cooled CCD (Andor Technology). Accuracy of Raman measurements is within  $\pm 0.2 \text{ cm}^{-1}$ . Raman spectra at high pressures and temperatures up to 450 K were obtained by heating the sample with a ring heater. In addition, the high temperature experiments were also carried out up to 1100 K by laser heating, and the temperature was measured using our earlier temperature-dependent studies.

XRD measurements of  $\text{TaVO}_5$  at ambient condition and retrieved from high pressure are recorded with  $\text{Mo K}\alpha$  with  $\lambda = 0.7107 \text{ \AA}$ . XPS was conducted in a photoelectron spectrometer using  $\text{Mg K}\alpha$  ( $h\nu = 1253.6 \text{ eV}$ ) as the primary excitation source. The sample chamber was

evacuated to a vacuum better than  $10^{-9}$  Torr. Photoelectron spectra were analyzed using a VG make CLAM2 analyzer system. The binding energies were calibrated with respect to the binding energy of O 1s at  $530.0 \text{ eV}$ .<sup>36</sup>

In the present study, oxidation states and local environments in  $\text{TaVO}_5$  before and after pressurizing have been investigated by XAS measurements, which include both extended X-ray absorption fine structure (EXAFS) and X-ray absorption near edge structure (XANES) measurements. XANES and EXAFS measurements were done at vanadium K edge using synchrotron radiation. For EXAFS and XANES measurements, powder samples of appropriate weights estimated to obtain a reasonable edge jump mixed with cellulose powder was pressed to pellets of 2.5 mm thick and 12.5 mm diameter prepared using an electrically operated hydraulic press.

XANES and EXAFS measurements of the samples at vanadium K edge were carried out at the Scanning EXAFS beamline (BL-9) at the Indus-2 Synchrotron Source (2.5 GeV, 100 mA) at the Raja Ramanna Centre for Advanced Technology (RRCAT), Indore, India.<sup>37,38</sup> The beamline covers a photon energy range of 4–25 keV and has a resolution of 1 eV at 10 keV. The XANES spectra of the samples and two reference samples  $\text{VOSO}_4$  and  $\text{V}_2\text{O}_5$  for 100%  $\text{V}^{+4}$  and  $\text{V}^{+5}$ , respectively, were recorded in the energy range 5420–5550 eV. The EXAFS spectra of the samples at vanadium K edge were recorded in the energy range 5400–6150 eV.

## RESULTS AND DISCUSSIONS

$\text{TaVO}_5$  is a corner-linked open framework structured compound. It is made up of corner-linked  $\text{TaO}_6$  octahedra and  $\text{VO}_4$  tetrahedra. Each  $\text{TaO}_6$  octahedra is linked to two  $\text{TaO}_6$  octahedra and four  $\text{VO}_4$  tetrahedra, and each  $\text{VO}_4$  tetrahedra is linked to four  $\text{TaO}_6$  octahedra.<sup>27</sup> At ambient conditions,  $\text{TaVO}_5$  crystallizes in orthorhombic structure with space group  $Pnma$  ( $D_{2h}^{16}$ ).

In the recent high pressure Raman studies of  $\text{TaVO}_5$ , we have observed a reversible structural phase transition at 0.2 GPa. It was also noted that features observed in the Raman spectra of the first high pressure phase are similar to that of Raman spectra of the low temperature monoclinic phase of  $\text{TaVO}_5$ . In Figure 1, we compare the Raman spectra of ambient

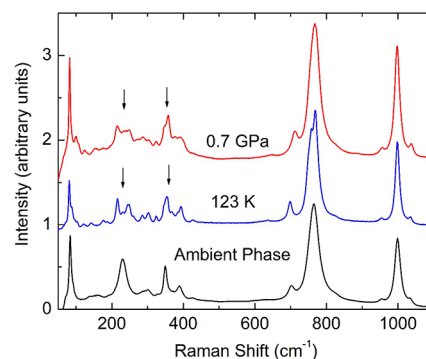


**Figure 1.** Comparison of Raman spectrum of  $\text{TaVO}_5$  in the orthorhombic phase, in the low temperature monoclinic phase at 123 K, and in the monoclinic phase at 0.7 GPa. Arrows indicate similar splitting of  $230$  and  $349 \text{ cm}^{-1}$  modes at low temperature and at high pressures.

orthorhombic phase  $\text{TaVO}_5$  with low temperature monoclinic phase at 123 K and with high pressure phase at 0.7 GPa, likely to be of monoclinic structure. Arrows indicate similar splitting of  $230$  and  $349 \text{ cm}^{-1}$  modes at low temperature and at high pressures. For orthorhombic phase of  $\text{TaVO}_5$ , 81 zone center optic phonon modes are expected as  $\Gamma_{\text{optic}} = 11A_g + 7B_{1g} + 11B_{2g} + 7B_{3g} + 10A_u + 13B_{1u} + 9B_{2u} + 13B_{3u}$ . Among these,  $A_g$

$B_{1g}$ ,  $B_{2g}$ , and  $B_{3g}$  are Raman active, while  $A_u$ ,  $B_{1u}$ ,  $B_{2u}$ , and  $B_{3u}$  are infrared active; whereas in monoclinic phase of  $\text{TaVO}_5$ , 165 zone center optic phonon modes are expected as  $\Gamma_{\text{optic}} = 42A_g + 42B_g + 41A_u + 40B_u$ . Among these,  $A_g$  and  $B_g$  are Raman active, while  $A_u$  and  $B_u$  are infrared active. Changes across the transition to the monoclinic phase are primarily reflected in the V–O related modes as a consequence of  $\text{VO}_4$  tetrahedra, which become irregular in the monoclinic phase, and a transformed low temperature phase has been reported to exhibit positive thermal expansion (PTE). Assuming the same structural phase transition with decreasing temperature as well as increasing pressure, the said structural phase transition can be concluded as a volume driven effect. A similar kind of reciprocal relationship between pressure and temperature dependent structural transitions was seen for several orthotungstates where transition from tetragonal scheelite structure to monoclinic fergusonite structure were observed.<sup>39</sup>

### High Pressure Neutron Diffraction Studies on $\text{TaVO}_5$

Earlier high pressure Raman studies confirmed that the ambient condition orthorhombic phase of  $\text{TaVO}_5$  undergoes a structural phase transition at 0.2 GPa to a possible monoclinic phase, which persists up to 8 GPa, above which  $\text{TaVO}_5$  undergoes PIA.<sup>30</sup> From high pressure Raman studies we know that  $\text{TaVO}_5$  remains in the first high pressure phase for pressure range 0.2 to 8 GPa, which was speculated to be of monoclinic structure. However, this speculation of monoclinic structure was purely based on comparison of changes observed in Raman spectra across temperature- and pressure-dependent studies, also discussed in Figure 1. Spectroscopic evidence are not enough to confirm the structure; hence, it was important to establish the structure of first high pressure phase using a diffraction technique. Changes across the orthorhombic to monoclinic transition predominantly involve distortion of the oxygen network and thus are expected to be more clearly distinguishable by neutron diffraction as compared to X-ray diffraction. So, we have carried out high pressure neutron diffraction experiment on  $\text{TaVO}_5$  up to 0.5 GPa. Figure 2 shows the

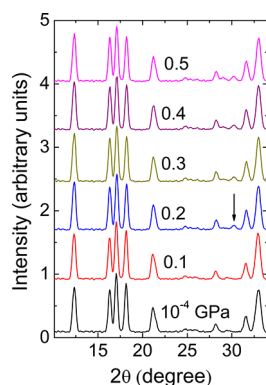


**Figure 2.** Neutron diffraction patterns of  $\text{TaVO}_5$  at different pressures. Arrow shows the new peak corresponding to high pressure phase.

neutron diffraction patterns of sample after all corrections in the given  $2\theta$  range. Figure 2 shows the neutron diffraction patterns of sample after all corrections in the given  $2\theta$  range. The arrow in Figure 2 shows the new peak that emerges around  $2\theta$  angle  $30.3^\circ$  and  $30.9^\circ$ , corresponding to the high pressure monoclinic phase. It confirms the orthorhombic to monoclinic structural transition observed in high pressure Raman spectroscopic experiments at 0.2 GPa. We have carried out

Rietveld refinement of neutron diffraction data. Figure 3 shows the Rietveld refinement pattern of  $\text{TaVO}_5$  at ambient condition

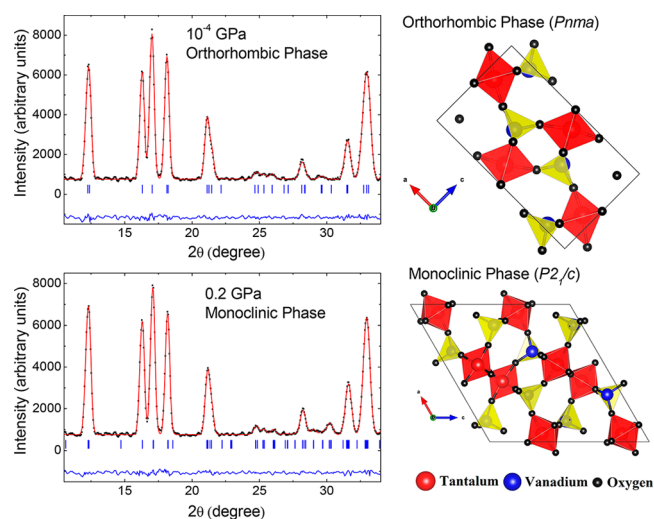


**Figure 3.** Rietveld refinement of neutron diffraction data of  $\text{TaVO}_5$  and crystal structures of orthorhombic ( $Pnma$ ) and monoclinic ( $P2_1/c$ ) phases of  $\text{TaVO}_5$ .

and at 0.2 GPa. It can be seen that the newly emerged peak at around  $30^\circ$  above 0.2 GPa are indexed by monoclinic phase ( $P2_1/c$ ). Hence, our high pressure neutron diffraction studies confirm that the high pressure phase has a monoclinic structure space group  $P2_1/c$ . Atomic positions of ambient orthorhombic and high pressure monoclinic structure, along with lattice parameters and unit cell volume are provided in Table 1. The crystal structures of orthorhombic and monoclinic phase are shown in Figure 3. As 0.5 GPa was the maximum pressure limit of experimental set up used for high pressure neutron diffraction studies, we could not carry out high pressure neutron diffraction studies beyond 0.5 GPa. However, results presented here are sufficient to prove the monoclinic phase of  $\text{TaVO}_5$  above 0.2 GPa.

**Pressure Induced Amorphization in  $\text{TaVO}_5$ .** Although insufficient kinetics has been attributed as the cause of PIA, the reason for amorphization in  $\text{TaVO}_5$  is puzzling; as for the amorphous phase, it is difficult to speculate whether the kinetics were insufficient either for phase transition or for decomposition. To address the issue, we have used the model suggested by Arora for PID, according to which PID is favorable if the total volume of daughter compounds are less than the parent compound.<sup>5</sup> This model is quite useful to predict the cause of PIA.

For  $\text{TaVO}_5$ , the possible decomposition reaction is  $\text{TaVO}_5 \rightarrow \text{Ta}_2\text{O}_5 + \text{V}_2\text{O}_5$ . The change in volume on decomposition can be written as

$$\Delta V = V_D - V_p$$

where  $V_D$  is the volume of the daughter compound and  $V_p$  is the volume of the parent compound at amorphization pressure. If  $\Delta V$  is negative, then amorphization is favorable due to PID. In the case of  $\text{TaVO}_5$ , PIA takes place around 8 GPa; hence, we have compared volumes of parent and daughter compounds at 8 GPa.  $\Delta V$  for the  $\text{TaVO}_5$  comes out to be about  $-26\%$ , which implies that PID is favorable in the case of  $\text{TaVO}_5$ , and PIA observed above 8 GPa could be due to insufficient kinetics required for PID. One of the daughter compounds,  $\text{V}_2\text{O}_5$  can

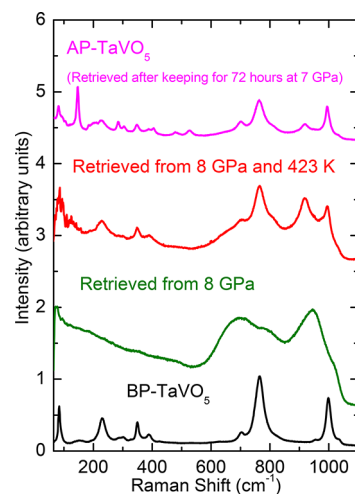
**Table 1. Structural Parameters for Orthorhombic and Monoclinic Phase of TaVO<sub>5</sub> at Ambient Conditions and 0.2 GPa, Respectively**

at ambient condition, orthorhombic; space group <i>Pnma</i>				
$a = 11.8559(17) \text{ \AA}, b = 5.5110(9) \text{ \AA}, c = 6.9317(12) \text{ \AA},$				
$V = 452.9(1) \text{ \AA}^3$				
atom	Wyckoff	$x/a$	$y/b$	$z/c$
Ta	4a	0.559(1)	0.25	0.158(2)
V	4c	0.348	0.25	0.524
O1	4b	0	0	0.5
O2	8d	0.124(7)	-0.003(2)	0.159(2)
O3	4c	0.703(1)	0.25	0.025(2)
O4	4c	0.923(1)	0.25	0.178(2)
at 0.2 GPa, monoclinic; space group <i>P2<sub>1</sub>/c</i>				
$a = 13.7404(12) \text{ \AA}, b = 5.4928(8) \text{ \AA}, c = 13.8141(9) \text{ \AA}, \beta = 120.13(1)^\circ$				
$V = 901.7(1) \text{ \AA}^3$				
atom	Wyckoff	$x/a$	$y/b$	$z/c$
Ta1	4e	0.439(2)	0.259(4)	0.291(2)
Ta2	4e	0.941(2)	0.255(5)	0.139(2)
V1	4e	0.150	0.216	0.051
V2	4e	0.657	0.265	0.092
O1	4e	0.004(2)	-0.025(3)	0.240(4)
O2	4e	0.505(2)	0.483(9)	0.241(2)
O3	4e	0.875(4)	0.026(8)	0.005(7)
O4	4e	0.882(1)	0.539(7)	0.035(5)
O5	4e	0.380(2)	0.522(7)	0.350(9)
O6	4e	0.368(8)	0.035(8)	0.362(9)
O7	4e	0.802(7)	0.241(4)	0.137(9)
O8	4e	0.292(6)	0.246(4)	0.158(9)
O9	4e	0.578(8)	0.251(8)	0.447(5)
O10	4e	0.070(2)	0.270(4)	0.121(9)

have  $\alpha$  or  $\beta$  phase, while parent compound TaVO<sub>5</sub> at high pressures is likely to have a monoclinic structure as per our previous discussion. With this assumption also the  $\Delta V$  comes out to be negative; hence, PID is strongly favorable in TaVO<sub>5</sub> under pressure. Due to PIA, the final phase or decomposed products remain speculative. If we provide the kinetics externally, then the compound may possibly transform to its final phase. We can provide kinetics intentionally either by providing heat or sufficient time under pressure. In the case of TaVO<sub>5</sub>, we have heated the sample at 423 K for 2 h at 8 GPa pressure and then recorded the Raman spectra of the HP-HT retrieved sample. For other possible ways of providing kinetics, we have kept the sample under 7 GPa pressure for 72 h and then carried out various measurements on the pressure retrieved sample. The pressure retrieved TaVO<sub>5</sub> sample is named as AP-TaVO<sub>5</sub>, while the unpressurized sample is named as BP-TaVO<sub>5</sub> in further discussion.

Irreversible PIA is observed above 8 GPa, which is confirmed by the fwhm of V–O symmetric and asymmetric stretching modes increasing to five times their fwhm at ambient conditions as shown in Figure 8 of ref 29. In the ambient condition orthorhombic structure of TaVO<sub>5</sub>, tantalum is six-coordinated, while vanadium is four-coordinated. In ambient condition Raman spectra, as shown in Figure 1, the modes in the frequency range 900–1050 cm<sup>-1</sup> are due to the symmetric stretching ( $\nu_1$ ), and those in 650–850 cm<sup>-1</sup> are due to asymmetric stretching ( $\nu_3$ ) modes of the VO<sub>4</sub> unit. The modes in the frequency range 200–450 cm<sup>-1</sup> have been assigned to bending modes of VO<sub>4</sub> tetrahedron. Modes below 200 cm<sup>-1</sup> are

lattice modes. Raman spectra of vanadates with tetrahedral coordination are well reported in the literature.<sup>40,41</sup> In Figure 4,

**Figure 4.** Raman spectra of BP-TaVO<sub>5</sub>, AP-TaVO<sub>5</sub>, and pressure retrieved TaVO<sub>5</sub> sample from DAC with and without heating.

we have shown the Raman spectra of BP-TaVO<sub>5</sub> (unpressurized sample), AP-TaVO<sub>5</sub> (sample retrieved after keeping for 72 h at 7 GPa), sample retrieved after DAC experiment at 8 GPa pressures (without heating), and sample retrieved after simultaneous pressure and heating at 8 GPa and 423 K. Raman spectra of TaVO<sub>5</sub> retrieved from 8 GPa without heating shows very broad peaks appearing only in the high frequency stretching mode region around 700, 793, and 945 cm<sup>-1</sup>; further, we did not observe any low frequency Raman modes, which confirms the irreversibility of PIA from 8 GPa. Broad modes around 700 and 945 cm<sup>-1</sup> observed in the stretching mode region correspond to asymmetric and symmetric stretching modes, respectively. These broad modes are less by almost 60 cm<sup>-1</sup> compared to its corresponding modes in ambient phase, indicating softening behavior, which could be due to an increase in coordination. In addition to this, a new broad mode is observed around 793 cm<sup>-1</sup>. These broad modes could be corresponding to higher coordination of vanadium. Under pressure, it may be possible that TaVO<sub>5</sub> attempts either to transform to a phase where vanadium has a higher coordination number like five or six coordination or to decompose into the compounds where vanadium has more than four coordinations; but because of insufficient kinetics, amorphization takes place. Evidence of the higher coordination of vanadium by Raman spectroscopy is consistent for PID as one of the possible decomposition products,  $\alpha$ -V<sub>2</sub>O<sub>5</sub>/ $\beta$ -V<sub>2</sub>O<sub>5</sub>, has vanadium with more than four coordinations.

Upon heating at high pressures, Raman spectra of TaVO<sub>5</sub> retrieved from simultaneous 8 GPa and 423 K show a few modes in bending and stretching mode regions, which are similar to those present in ambient conditions of TaVO<sub>5</sub>. In addition to the ambient phase modes, a new mode appearing around 920 cm<sup>-1</sup> could be due to higher coordination of vanadium. However, from the Raman spectra shown in Figure 4, it is difficult to conclude whether it is due to a new phase of TaVO<sub>5</sub> or decomposition under pressure. Raman spectra also show signatures of tetrahedral coordination of vanadium due to the presence of ambient phase. It may be noted that  $\beta$ -V<sub>2</sub>O<sub>5</sub> has its intense peak around 930 cm<sup>-1</sup>.<sup>42,43</sup>

Raman spectra of the AP-TaVO<sub>5</sub> sample shown in Figure 4 give an additional Raman peak around 920 cm<sup>-1</sup> compared to BP-TaVO<sub>5</sub>, similar to that observed for the TaVO<sub>5</sub> sample retrieved after simultaneous pressure and heating. This may be due to higher coordination of vanadium, and possibly the lower oxidation state could be due to partial reduction of V<sup>5+</sup>.

**XRD Measurement on Pressure Retrieved TaVO<sub>5</sub>.** To understand the changes observed in Raman studies, we have carried out XRD measurements of BP-TaVO<sub>5</sub> and AP-TaVO<sub>5</sub> samples, and they are shown in Figure 5. In the AP-TaVO<sub>5</sub>

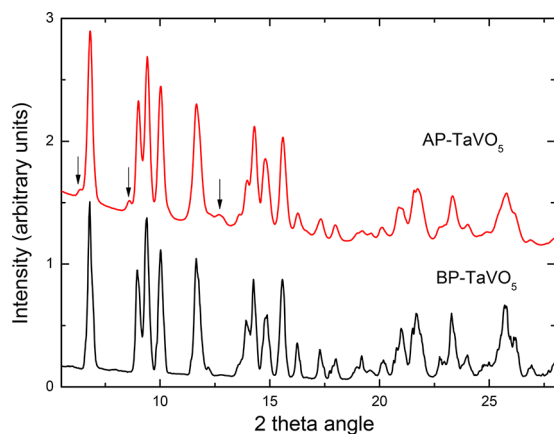


**Figure 5.** X-ray diffraction patterns of BP-TaVO<sub>5</sub> and AP-TaVO<sub>5</sub>. Arrows indicate new peaks emerging in AP-TaVO<sub>5</sub>.

XRD pattern, new peaks at  $2\theta$  around 6.3°, 8.6°, and 12.7° are observed, shown with arrows in Figure 5, which were otherwise absent in BP-TaVO<sub>5</sub>. Positions of these new peaks correspond to  $\beta$ -V<sub>2</sub>O<sub>5</sub>,<sup>44</sup> which could be one of the decomposed products.

**XPS and XAS Measurement on Pressure Retrieved TaVO<sub>5</sub>.** Structural phase transitions in materials are mainly manifested in the form of change in atomic coordination and/or by change in oxidation state. We have carried out XPS measurement on BP-TaVO<sub>5</sub> and AP-TaVO<sub>5</sub> in order to understand the change in oxidation state of vanadium after pressurizing. Figure 6 shows the XPS spectra of BP-TaVO<sub>5</sub> and AP-TaVO<sub>5</sub> for vanadium 2p<sub>3/2</sub>, which were recorded in order to

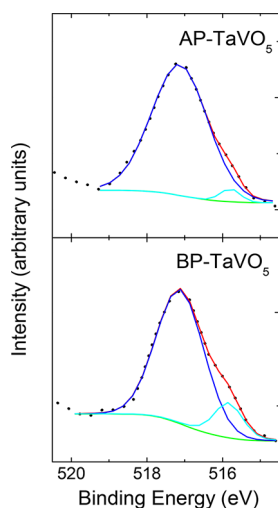


**Figure 6.** XPS spectra of BP-TaVO<sub>5</sub> and AP-TaVO<sub>5</sub> for vanadium 2p<sub>3/2</sub>.

identify the oxidation states of vanadium present in BP-TaVO<sub>5</sub> and AP-TaVO<sub>5</sub>. In both samples, binding energy of vanadium 2p<sub>3/2</sub> corresponding to +5 oxidation states is found to be 517.1 eV, which is in agreement with literature values.<sup>37,38</sup> In both samples, an additional peak corresponding to a small contribution from the +4 oxidation state of vanadium 2p<sub>1/2</sub> is observed at 515.8 eV. We have found that there is no considerable change in oxidation state due to pressure.

We have also investigated the oxidation state of vanadium using a synchrotron based XANES technique. The XANES spectra of the BP-TaVO<sub>5</sub> and AP-TaVO<sub>5</sub> samples at the vanadium K edge along with that of the reference samples of VOSO<sub>4</sub> and V<sub>2</sub>O<sub>5</sub> are shown in Figure 7. From the figure, it can

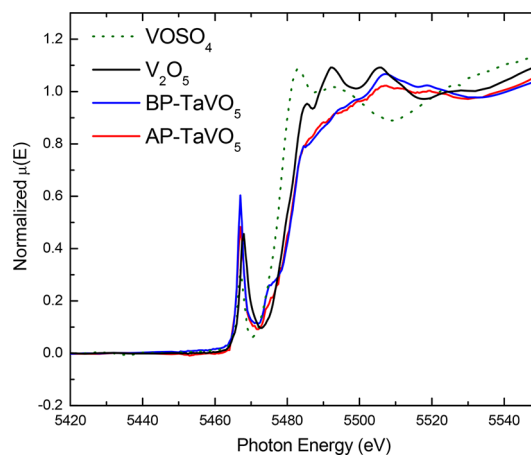


**Figure 7.** XANES spectra of the BP-TaVO<sub>5</sub> and AP-TaVO<sub>5</sub> at vanadium K edge.

be seen that the absorption edge of the BP-TaVO<sub>5</sub> and AP-TaVO<sub>5</sub> samples are close to the absorption edge of the V<sub>2</sub>O<sub>5</sub> reference sample, which confirms that the vanadium ions in TaVO<sub>5</sub> samples before and after pressurizing remain in +5 oxidation state. This observation is consistent with XPS measurements.

We have carried out EXAFS investigation on BP-TaVO<sub>5</sub> and AP-TaVO<sub>5</sub> to understand the change in coordination of vanadium and also possible decomposed product. Experimental EXAFS spectra of the BP-TaVO<sub>5</sub> and AP-TaVO<sub>5</sub> samples measured at the vanadium K-edge are shown in Figure 8a. The data reduction to obtain the  $\chi(k)$  vs  $k$  plots and subsequently the radial distribution function  $\chi(R)$  versus  $R$  plots were obtained from the measured  $\mu(E)$  versus  $E$  spectra and have been carried out following the standard procedures<sup>45,46</sup> using IFEFFIT software package.<sup>47</sup> The  $\chi(R)$  versus  $R$  plot or the Fourier transformed (FT) EXAFS spectrum of the BP-TaVO<sub>5</sub> sample at the vanadium K edge has been fitted with a theoretical spectrum assuming orthorhombic TaVO<sub>5</sub> structure with space group *Pnma*, in which vanadium has four coordination. However, when the experimental spectra of the AP-TaVO<sub>5</sub> sample was attempted to fit with the orthorhombic TaVO<sub>5</sub> structure, it resulted in lower coordination of the vanadium ions than BP-TaVO<sub>5</sub>. This could be due to the presence of mixed phase in the sample, which is already suggested by Raman and XRD measurement of the pressure retrieved TaVO<sub>5</sub> sample. This is a similar situation as  $\beta$ -V<sub>2</sub>O<sub>5</sub> where VO<sub>6</sub> polyhedra is highly distorted with three shorter V–O and three longer bonds.<sup>48</sup> The EXAFS spectra of the AP-TaVO<sub>5</sub> sample has then been fitted by assuming linear

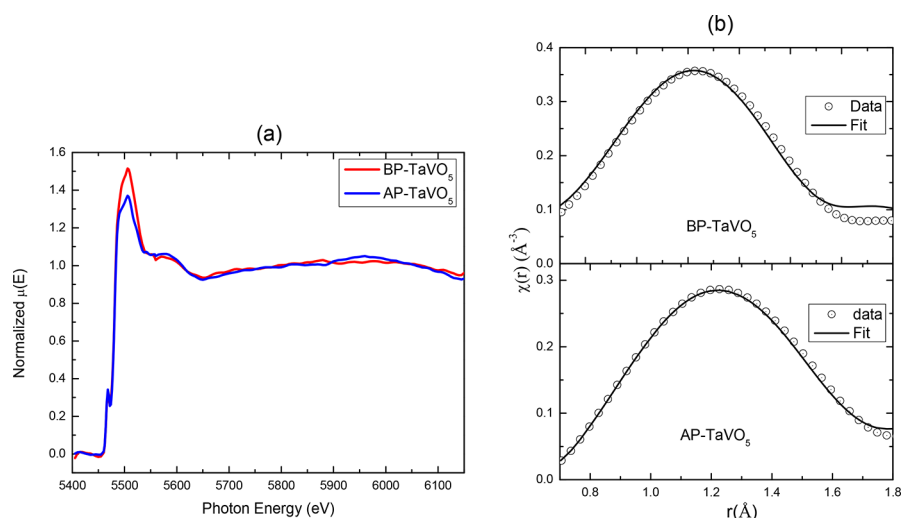


**Figure 8.** (a) EXAFS spectra of the BP-TaVO<sub>5</sub> and AP-TaVO<sub>5</sub> samples measured at vanadium K-edge. (b) Experimental EXAFS spectra at vanadium K-edge fitted with theoretical plots.

combination of the orthorhombic TaVO<sub>5</sub> structure and monoclinic  $\beta$ -V<sub>2</sub>O<sub>5</sub> structure with space group  $P2_1/m$ . The TaVO<sub>5</sub> structure is represented by the two different V–O shells, and the  $\beta$ -V<sub>2</sub>O<sub>5</sub> structure is represented by four different V–O shells as shown in Table 2. While fitting the experimental

**Table 2.** EXAFS Fitting Results at Vanadium K Edge

R factor = 0.007	theoretical		experimental BP-TaVO <sub>5</sub>			
	<i>r</i> (Å)	<i>N</i>	<i>r</i> (Å)	<i>N</i>	$\sigma^2$	
	V–O1	1.64	2	1.65	2	0.0043
	V–O2	1.70	2	1.70	2	0.0031
R factor = 0.004	theoretical		experimental AP-TaVO <sub>5</sub>			
	<i>r</i> (Å)	<i>N</i>	<i>r</i> (Å)	<i>N</i>	$\sigma^2$	
	TaVO <sub>5</sub> Structure (85%)					
	V–O1	1.64	2	1.69	2	0.0031
	V–O2	1.70	2	1.71	2	0.0036
	$\beta$ -V <sub>2</sub> O <sub>5</sub> Structure (15%)					
	V1–O1	1.55	1	1.58	1	0.002
	V2–O1	1.67	2	1.68	2	0.001
	V1–O2 and V2–O2	1.90	4(2 + 2)	1.94	4	0.0045
	V1–O3	1.99	2	2.01	2	0.002

data, the coordination of the shells are kept the same as their theoretical values; only the percentage of the two phases are varied to get a good fit. Figures 8b shows experimental spectra along with best fit theoretical plots, and the values of the best fit parameters are given in Table 2. The best fitting of the experimental spectra suggests the presence of 85% TaVO<sub>5</sub> and 15%  $\beta$ -V<sub>2</sub>O<sub>5</sub> phase in AP-TaVO<sub>5</sub>. Also, from Table 2, it can be seen that the bond lengths of the V–O bonds of the TaVO<sub>5</sub> phase increase after pressurizing.

From the above experiments carried out on pressure retrieved TaVO<sub>5</sub>, we can conclude that kinetic hindrance of PID could be the possible reason for PIA observed in TaVO<sub>5</sub>. This integrated study using Raman spectroscopy, XRD, EXAFS, XANES, and XPS indicates that PIA in TaVO<sub>5</sub> is due to hindrance in PID.

**Temperature–Pressure Phase Diagram of TaVO<sub>5</sub>.** In our earlier work, we have observed local heating in TaVO<sub>5</sub> with the variation of laser power.<sup>30</sup> We have estimated the sample

temperature with respect to laser power, from the shift in peak position with respect to laser power and temperature-dependent shift in peak position at constant minimum power. Error in estimation of temperature is about  $\pm 50$  K. The laser power of 100 mW in open air has resulted in phase transition of TaVO<sub>5</sub>. This laser power corresponds to  $\sim 1120$  K. Resultant spectra of TaVO<sub>5</sub> is shown in Figure 9. This could be a

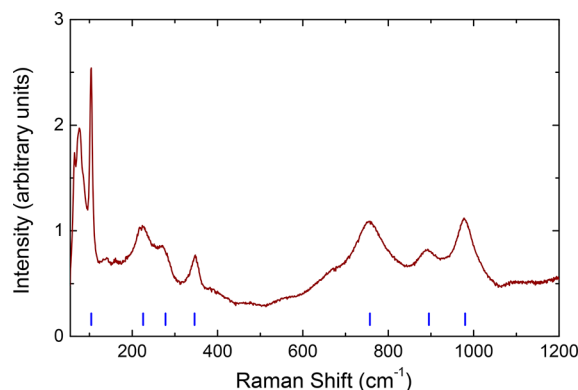


**Figure 9.** Raman spectra of TaVO<sub>5</sub> at 100 mW laser power. Blue tick marks indicate positions of prominent Raman modes.

tetragonal phase of TaVO<sub>5</sub>.<sup>27</sup> In order to obtain the pressure–temperature phase relationship of TaVO<sub>5</sub>, we have heated the sample inside the DAC using different laser powers. Laser heating inside DAC has been used several times for estimating phase relations.<sup>49</sup> We have determined the stability of the high pressure phase as a function of temperature up to 1170 K and have constructed the phase diagram. The critical pressure for transition to monoclinic phase is 0.2 GPa at  $T = 300$  K, and it increases linearly with increasing temperature to become 0.7 GPa at 1170 K. The temperature–pressure phase relationship obtained for TaVO<sub>5</sub> is given in Figure 10. The slope of the phase boundary is called a Clapeyron slope given as  $\frac{dP}{dT} = \frac{\Delta S}{\Delta V}$  where  $P$ ,  $T$ ,  $S$  and  $V$  represent pressure, temperature, entropy, and volume, respectively. The Clapeyron slope of orthorhombic to monoclinic phase boundary is positive ( $dP/dT = 0.0007(1)$  GPa K<sup>−1</sup>), while the monoclinic to amorphous phase boundary Clapeyron slope is found to be negative. Pressure at

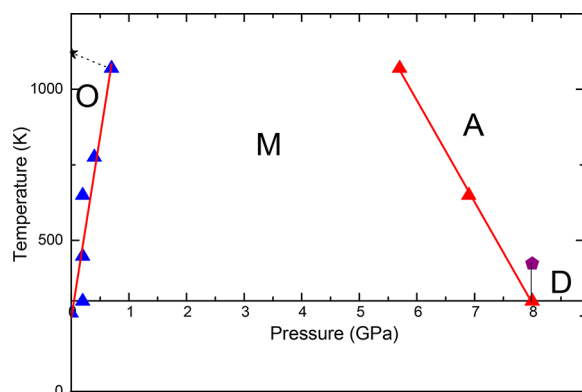


**Figure 10.** Temperature–pressure phase relationship of TaVO<sub>5</sub>. Black star mark represents possible tetragonal phase [symbols: O, orthorhombic phase (*Pnma*); M, monoclinic phase (*P*<sub>21</sub>/*c*); A, amorphous phase; D, decomposition].

which the compound becomes completely amorphous decreases with an increase in temperature. As entropy is a function of pressure as well as temperature, it always increases with temperature, while with pressure, it may decrease or increase. For positive thermal expansion material entropy should decrease with pressure, and for NTE materials, it should increase with pressure.<sup>50</sup> Positive Clapeyron slope across orthorhombic to monoclinic phase boundary could be due to NTE nature of TaVO<sub>5</sub> in orthorhombic phase. Negative Clapeyron slope at monoclinic to amorphous phase boundary could be due to higher entropy in amorphous phase compared to monoclinic phase.

## SUMMARY

From *in situ* high pressure neutron diffraction, a monoclinic lattice with space group *P*<sub>21</sub>/*c* is assigned for structure of high pressure phase of TaVO<sub>5</sub>. We have also presented a comprehensive study of PIA in TaVO<sub>5</sub> using *ex situ* Raman, XRD, XPS, and XAS measurements. We have found that the underlying mechanism behind PIA observed in TaVO<sub>5</sub> is due to the kinetic hindrance of PID of TaVO<sub>5</sub> to β-V<sub>2</sub>O<sub>5</sub> and probably Ta<sub>2</sub>O<sub>5</sub>. We have also experimentally mapped the phase diagram of TaVO<sub>5</sub> by laser heating at high pressures in a diamond anvil cell.

## AUTHOR INFORMATION

### Corresponding Author

\*E-mail: rekhar@barc.gov.in.

### ORCID

Rekha Rao: 0000-0002-1848-6171

Srungarpu Nagabhusan Achary: 0000-0002-2103-1063

Alka B. Garg: 0000-0003-4050-8469

### Present Address

#Center for High Pressure Science and Technology Advanced Research (HPSTAR), Shanghai 201203, China.

### Notes

The authors declare no competing financial interest.

## REFERENCES

- (1) Sharma, S. M.; Sikka, S. K. Pressure induced amorphization of materials. *Prog. Mater. Sci.* **1996**, *40*, 1–77.
- (2) Maczka, M.; Souza Filho, A. G.; Paraguassu, W.; Freire, P. T. C.; Mendes Filho, J.; Hanuza, J. Pressure-induced structural phase

transitions and amorphization in selected molybdates and tungstates. *Prog. Mater. Sci.* **2012**, *57*, 1335–1381.

(3) Lind, C. Two Decades of Negative Thermal Expansion Research: Where Do We Stand? *Materials* **2012**, *5*, 1125–1154.

(4) Machon, D.; Meersman, F.; Wilding, M. C.; Wilson, M.; McMillan, P. F. Pressure-induced amorphization and polyamorphism: Inorganic and biochemical systems. *Prog. Mater. Sci.* **2014**, *61*, 216–282.

(5) Arora, A. K. Pressure-induced amorphization versus decomposition. *Solid State Commun.* **2000**, *115*, 665–668.

(6) Tse, J. S.; Klug, D. D.; Tulk, C. A.; Swainson, I.; Svensson, E. C.; Loong, C. K.; Shpakov, V.; Belosludov, V. R.; Belosludov, R. V.; Kawazoe, Y. The mechanisms for pressure-induced amorphization of ice Ih. *Nature* **1999**, *400*, 647–649.

(7) Narayanan, B.; Reimanis, I. E.; Ciobanu, C. V. Atomic-scale mechanism for pressure-induced amorphization of β-eucryptite. *J. Appl. Phys.* **2013**, *114* (8), 083520.

(8) Speedy, R. J. Models for the amorphization of compressed crystals. *J. Phys.: Condens. Matter* **1996**, *8*, 10907.

(9) Mishima, O.; Calvert, L. D.; Whalley, E. ‘Melting ice’ I at 77 K and 10 kbar: a new method of making amorphous solids. *Nature* **1984**, *310*, 393–395.

(10) Hemley, R. J.; Jephcoat, A. P.; Mao, H. K.; Ming, L. C.; Manghnani, M. H. Pressure-induced amorphization of crystalline silica. *Nature* **1988**, *334*, 52–54.

(11) Kruger, M. B.; Jeanloz, R. Memory Glass: An Amorphous Material Formed from AlPO<sub>4</sub>. *Science* **1990**, *249*, 647–649.

(12) Li, Y.; Tang, R.; Li, N.; Li, H.; Zhao, X.; Zhu, P.; Wang, X. Pressure-induced amorphization of metavanadate crystals SrV<sub>2</sub>O<sub>6</sub> and BaV<sub>2</sub>O<sub>6</sub>. *J. Appl. Phys.* **2015**, *118* (3), 035902.

(13) Wang, Y.; Zhu, J.; Yang, W.; Wen, T.; Pravica, M.; Liu, Z.; Hou, M.; Fei, Y.; Kang, L.; Lin, Z.; Jin, C.; Zhao, Y. Reversible switching between pressure-induced amorphization and thermal-driven recrystallization in VO<sub>2</sub>(B) nanosheets. *Nat. Commun.* **2016**, *7*, 12214.

(14) Silva Santos, S. D.; Paraguassu, W.; Maczka, M.; Freire, P. T. C. High pressure Raman scattering study on Sm<sub>2</sub>Mo<sub>4</sub>O<sub>15</sub> system. *Spectrochim. Acta, Part A* **2017**, *174*, 80–85.

(15) Errandonea, D.; Somayazulu, M.; Häusermann, D. Phase transitions and amorphization of CaWO<sub>4</sub> at high pressure. *Phys. Status Solidi B* **2002**, *235* (1), 162–169.

(16) Arora, A. K. Amorphous polymorphs. *AIP Conf. Proc.* **2011**, *1447*, 51–54.

(17) Deb, S. K.; Wilding, M.; Somayazulu, M.; McMillan, P. F. Pressure-induced amorphization and an amorphous-amorphous transition in densified porous silicon. *Nature* **2001**, *414*, 528–530.

(18) Arora, A. K.; Tomoko, S.; Takehiko, Y. Quenchable high-density amorphous polymorphs of zirconium tungstate. *J. Phys.: Condens. Matter* **2011**, *23*, 112207.

(19) Arora, A. K.; Sato, T.; Okada, T.; Yagi, T. High-pressure amorphous phase of vanadium pentoxide. *Phys. Rev. B: Condens. Matter Mater. Phys.* **2012**, *85*, 094113.

(20) Wang, J.; Cui, Q.; Hu, T.; Yang, J.; Li, X.; Liu, Y.; Liu, B.; Zhao, W.; Zhu, H.; Yang, L. Pressure-Induced Amorphization in BaF<sub>2</sub> Nanoparticles. *J. Phys. Chem. C* **2016**, *120*, 12249–12253.

(21) Perottoni, C. A.; Jornada, J. A. H. d. Pressure-Induced Amorphization and Negative Thermal Expansion in ZrW<sub>2</sub>O<sub>8</sub>. *Science* **1998**, *280*, 886–889.

(22) Varga, T.; Wilkinson, A. P.; Jupe, A. C.; Lind, C.; Bassett, W. A.; Zha, C.-S. Pressure-induced amorphization of cubic ZrW<sub>2</sub>O<sub>8</sub> studied *in situ* and *ex situ* by synchrotron x-ray diffraction and absorption. *Phys. Rev. B: Condens. Matter Mater. Phys.* **2005**, *72*, 024117.

(23) Varga, T.; Wilkinson, A. P. Zirconium coordination change upon the pressure-induced amorphization of cubic ZrW<sub>2</sub>O<sub>8</sub> and ZrMo<sub>2</sub>O<sub>8</sub>. *Phys. Rev. B: Condens. Matter Mater. Phys.* **2009**, *79*, 224119.

(24) Rao, R.; Achary, S. N.; Tyagi, A. K.; Sakuntala, T. Raman spectroscopic study of high-pressure behavior of Ag<sub>3</sub>[Co(CN)<sub>6</sub>]. *Phys. Rev. B: Condens. Matter Mater. Phys.* **2011**, *84*, 054107.

- (25) Catafesta, J.; Rovani, P. R.; Perottoni, C. A.; Pereira, A. S. Pressure-enhanced decomposition of  $\text{Ag}_3[\text{Co}(\text{CN})_6]$ . *J. Phys. Chem. Solids* **2015**, *77*, 151–156.
- (26) Pereira, A. S.; Perottoni, C. A.; da Jornada, J. A. H. Raman spectroscopy as a probe for in situ studies of pressure-induced amorphization: some illustrative examples. *J. Raman Spectrosc.* **2003**, *34*, 578–586.
- (27) Wang, X.; Huang, Q.; Deng, J.; Yu, R.; Chen, J.; Xing, X. Phase Transformation and Negative Thermal Expansion in  $\text{TaVO}_5$ . *Inorg. Chem.* **2011**, *50*, 2685–2690.
- (28) Lü, X.; Hu, Q.; Yang, W.; Bai, L.; Sheng, H.; Wang, L.; Huang, F.; Wen, J.; Miller, D. J.; Zhao, Y. Pressure-Induced Amorphization in Single-Crystal  $\text{Ta}_2\text{O}_5$  Nanowires: A Kinetic Mechanism and Improved Electrical Conductivity. *J. Am. Chem. Soc.* **2013**, *135*, 13947–13953.
- (29) Li, Q.; Zhang, H.; Cheng, B.; Liu, R.; Liu, B.; Liu, J.; Chen, Z.; Zou, B.; Cui, T.; Liu, B. Pressure-induced amorphization in orthorhombic  $\text{Ta}_2\text{O}_5$ : An intrinsic character of crystal. *J. Appl. Phys.* **2014**, *115*, 193512.
- (30) Salke, N. P.; Gupta, M. K.; Rao, R.; Mittal, R.; Deng, J.; Xing, X. Raman and ab initio investigation of negative thermal expansion material  $\text{TaVO}_5$ : Insights into phase stability and anharmonicity. *J. Appl. Phys.* **2015**, *117*, 235902.
- (31) Krishna, P. S. R.; Shinde, A. B.; Vaidya, S. N.; Paranjpe, S. K. A compact piston-cylinder press for neutron scattering experiments. *Solid State Physics (India) India* **2001**, 21.
- (32) Krishna, P. S. R.; Shinde, A. B. A high throughput reactor based high-Q diffractometer for the structure of disordered materials. *Solid State Physics (India) India* **2002**, 121.
- (33) Petrillo, C.; Sacchetti, F. Analysis of neutron diffraction data in the case of high-scattering cells. *Acta Crystallogr., Sect. A: Found. Crystallogr.* **1990**, *46*, 440–449.
- (34) Jayaraman, A. Diamond anvil cell and high-pressure physical investigations. *Rev. Mod. Phys.* **1983**, *55*, 65–108.
- (35) Piermarini, G. J.; Block, S.; Barnett, J. D.; Forman, R. A. Calibration of the pressure dependence of the R1 ruby fluorescence line to 195 kbar. *J. Appl. Phys.* **1975**, *46*, 2774–2780.
- (36) Silversmit, G.; Depla, D.; Poelman, H.; Marin, G. B.; De Gryse, R. Determination of the V2p XPS binding energies for different vanadium oxidation states ( $\text{V}^{5+}$  to  $\text{V}^{0+}$ ). *J. Electron Spectrosc. Relat. Phenom.* **2004**, *135*, 167–175.
- (37) Poswal, A. K.; Agrawal, A.; Yadav, A. K.; Nayak, C.; Basu, S.; Kane, S. R.; Garg, C. K.; Bhattacharyya, D.; Jha, S. N.; Sahoo, N. K. Commissioning and first results of scanning type EXAFS beamline (BL-09) at INDUS-2 synchrotron source. *AIP Conf. Proc.* **2013**, *1591*, 649–651.
- (38) Basu, S.; Nayak, C.; Yadav, A. K.; Agrawal, A.; Poswal, A. K.; Bhattacharyya, D.; Jha, S. N.; Sahoo, N. K. A comprehensive facility for EXAFS measurements at the INDUS-2 synchrotron source at RRCAT, Indore, India. *Journal of Physics: Conference Series* **2014**, *493*, 012032.
- (39) Errandonea, D. Landau theory applied to phase transitions in calcium orthotungstate and isostructural compounds. *EPL (Europhysics Letters)* **2007**, *77*, 56001.
- (40) Errandonea, D.; Manjón, F. J.; Muñoz, A.; Rodríguez-Hernández, P.; Panchal, V.; Achary, S. N.; Tyagi, A. K. High-pressure polymorphs of  $\text{TbVO}_4$ : A Raman and ab initio study. *J. Alloys Compd.* **2013**, *577*, 327–335.
- (41) Panchal, V.; Errandonea, D.; Manjón, F. J.; Muñoz, A.; Rodríguez-Hernández, P.; Achary, S. N.; Tyagi, A. K. High-pressure lattice-dynamics of  $\text{NdVO}_4$ . *J. Phys. Chem. Solids* **2017**, *100*, 126–133.
- (42) Baddour-Hadjean, R.; Smirnov, M. B.; Smirnov, K. S.; Kazimirov, V. Y.; Gallardo-Amores, J. M.; Amador, U.; Arroyo-de Dompablo, M. E.; Pereira-Ramos, J. P. Lattice Dynamics of  $\beta\text{-V}_2\text{O}_5$ : Raman Spectroscopic Insight into the Atomistic Structure of a High-Pressure Vanadium Pentoxide Polymorph. *Inorg. Chem.* **2012**, *51*, 3194–3201.
- (43) Zibrov, I. P.; Filonenko, V. P.; Lyapin, S. G.; Sidorov, V. A. The high pressure phases  $\beta$ - and  $\delta\text{-V}_2\text{O}_5$ : structure refinement, electrical and optical properties, thermal stability. *High Pressure Res.* **2013**, *33*, 399–408.
- (44) JCPDS card number 451074.
- (45) Konigsberger, D. C.; Prince, R. *X-Ray Absorption: Principles, Applications, Techniques of EXAFS, SEXAFS and XANES*; Wiley: New York, 1988.
- (46) Kelly, S. D.; Hesterberg, D.; Ravel, B. *Analysis of Soils and Minerals Using X-ray Absorption Spectroscopy*; Soil Science Society of America: Madison, WI, 2008.
- (47) Newville, M.; Ravel, B.; Haskel, D.; Rehr, J. J.; Stern, E. A.; Yacoby, Y. Analysis of multiple-scattering XAFS data using theoretical standards. *Phys. B* **1995**, *208–209*, 154–156.
- (48) Balog, P.; Orosel, D.; Cancarevic, Z.; Schön, C.; Jansen, M.  $\text{V}_2\text{O}_5$  phase diagram revisited at high pressures and high temperatures. *J. Alloys Compd.* **2007**, *429*, 87–98.
- (49) Membreño, N.; Xiao, P.; Park, K.-S.; Goodenough, J. B.; Henkelman, G.; Stevenson, K. J. In Situ Raman Study of Phase Stability of  $\alpha\text{-Li}_3\text{V}_2(\text{PO}_4)_3$  upon Thermal and Laser Heating. *J. Phys. Chem. C* **2013**, *117*, 11994–12002.
- (50) Liu, Z.-K.; Wang, Y.; Shang, S. Thermal Expansion Anomaly Regulated by Entropy. *Sci. Rep.* **2015**, *4*, 7043.